seven day DMEM group n = 7) were injected into injured sites using glass micropipettes attached to a 10 μL Hamilton syringe (Hamilton Company, Reno, NV). The injection was made at a one millimeter depth over a period of one minute. The needle was left in the spinal cord for an additional two minutes following injection in order to minimize reflux. The sites of injection were at the lesion epicenter. All animals were immunosuppressed subcutaneously with cyclosporine A (10 mg/kg, Novartis, Basel, Switzerland) for 14 days immediately after cell transplantation or DMEM injection. Thereafter, cyclosporine (Neoral, Novartis) was mixed in drinking water at 50 μg/mL concentration until sacrifice. None of the animals showed abnormal behavior. All the experimental procedures were performed in compliance with the guidelines established by the Animal Care and Use Committee of Chiba University.

Assessment of sensory motor functions

BBB open field locomotor test

Hind limb function was assessed in an open field (100 × 60 cm plastic pool) using the BBB open field locomotor test.[2] Measurements were performed one week after contusion injury and weekly thereafter for eight weeks. Tests were videotaped for five minutes and scored by a trained observer who was unaware of the treatment group.

Inclined plane test

Eight weeks after SCI, animals were placed in a head up position on an inclined plane and the angle of the slope was gradually increased. The angle at which the animal fell down from the slope was recorded, with three trials per animal. The median values were compared between the astrocyte group and the DMEM group. We also performed the test with normal rats (n = 5).

SCANET test

We performed movement analysis using the SCANET MV-40 (Melquest, Toyama, Japan). Rats were allowed to move freely in the attached wide plastic box (460 mm x 460 mm x 303 mm (H)). The SCANET system consists of a cage equipped with two crossing infrared sensor frames arranged at different heights, by which small (M1) and large (M2) horizontal movements can be monitored. The authors assessed locomotor function by determining the M1 scores for five and 30 minutes. The quantity of two dimensional motions was accumulated automatically.[23]

Sensory tests

Thermal nociceptive thresholds in rat hind limbs were evaluated using a Hargreaves device (Ugo Basile, Varese, Italy). The rats were placed in individual transparent acrylic boxes with the floor maintained at 28°C. A heat stimulus (150 mcal/ s/ cm^2) was delivered using a 0.5 cm diameter radiant heat source positioned under the plantar surface of the hind limb. The heat source was placed alternately under each hind limb to avoid anticipation by the animal. A cutoff time of 22 seconds was used, as it had been ascertained that no tissue

damage would result within this time period. The withdrawal threshold was calculated as the average of six consecutive tests.

Mechanical withdrawal thresholds in rat hind limbs were tested using a dynamic plantar aesthesiometer (Ugo Basile), in which a mechanical stimulus was applied via an actuator filament (0.5 mm diameter), which under computer control applies a linear ramp 5.0 g/s to the plantar surface of the hind limb. The withdrawal threshold was calculated as the average of six consecutive tests. Both tests were performed eight weeks after contusion. For comparison with baseline, we also performed both tests with normal rats (n = 5).

Tissue preparation

For histological evaluation, eight weeks after SCI, all animals were perfused transcardially with 4% paraformaldehyde in PBS (pH 7.4) under pentobarbital anesthesia (50 mg/kg, Abbott Laboratories, IL). A tissue block of the spinal cord including the lesion epicenter (Th 9-11) was removed and treated overnight in the same fixative, stored in 20% sucrose in PBS at 4°C, embedded in OCT compound (Sakura Finetechnical, Tokyo, Japan) and frozen at -80°C. Spinal cords were freeze-mounted on a holder, cut into 25 μm sagittal or transverse sections, and placed on poly-L-lysine-coated glass slides. For midsagittal sections (three day astrocyte group, n = 10; seven day astrocyte group, n = 3), spinal cords (1.2 cm length centered upon the lesion) were sliced and mounted on six sequential slides. Each slide had 6 - 8 slices spaced at 150 μm intervals for each sequential section, which correspond to one millimeter spinal cord width. For cross sections of the spinal cords (three day astrocyte group, n = 10; three day DMEM group, n = 5; seven day astrocyte group, n = 6; seven day DMEM group, n = 6), we sliced 8.0 mm long spinal cord pieces centered on the lesion. Every third slice was mounted on six sequential slides. Each slide had 16 – 18 sequential sections spaced at 450 μm intervals, which corresponded to a seven to eight millimeter length of spinal cord.

Histological analyses

Transplanted cell counts

Sagittal sections of the spinal cords were used to estimate counts of viable transplanted cells eight weeks after SCI. The PKH28 red fluorescence was observed by fluorescence microscopy (DP71, Olympus, Tokyo, Japan). Three slices per animal were observed with a 10x objective lens. One slice was divided into four pictures. We counted twelve pictures for each animal and averaged the cell densities. When we counted surviving cells in the spinal cord, we assumed that the spinal cord was a 4.0 mm cylinder whose diameter averaged 0.92 mm. One cross section had an area of $\pi \cdot (0.46)^2$ mm^2. We hypothesized that the height of transplanted cells under these conditions was approximately 40 μm. If a spinal cord is assumed to be cylindrical, a 4.0 mm long spinal cord segment would be composed of 100 cross sections. If the surviving cell density is X cells/ mm^2 , then the surviving cell number in the 4.0 mm long

spinal cord is given by $100 \cdot (0.46)^2$ X cell number.

We analyzed transplanted cells for the presence of GFAP-positive astrocytes, Tuj-1-positive neurons, or GST-• -positive oligodendrocytes. We used mouse anti-GFAP antibody (1:400, Sigma-Aldrich), mouse anti-• -tubulin III antibody (1:800, Covance), and mouse anti- GST-• (1:1000, BD Pharmingen, Franklin Lakes, NJ) for primary antibodies, followed by Alexa-Fluor 488-conjugated anti-mouse IgG (1:800, Molecular Probes) for secondary antibody. We used LSM5 Pascal confocal laser scanning microscopy to observe double positive cells (Carl Zeiss, Oberkochen, Germany).

Luxol Fast Blue (LFB) staining

We performed LFB staining for the three day astrocyte group and the three day DMEM group to measure the area of spared white matter eight weeks after SCI. One slide per animal was stained with LFB for myelin staining. Slices were photographed using an optical microscope (DP71, Olympus) with a 4x objective lens. The percentage of spared white matter was calculated from the number of pixels representing the area of spared white matter divided by the number of pixels for total cross sectional area using Scion Image computer analysis software (Scion Corporation, Frederick, MA, USA). We calculated the data from three regions (the lesion epicenter, 2.5 mm rostral, and 2.5 mm caudal from the lesion epicenter).

Quantitative analysis of CGRP-positive area

For the three day astrocyte andthe DMEM group, one cross section per animal was incubated with rabbit anti-calcitonin gene related peptide (CGRP) antibody for overnight at 4°C (1:1000, ImmunoStar, Inc. Hudson, WI) and reacted with Alexa-Fluor 488 goat anti-rabbit IgG secondary antibody for one hours at room temperature. Three slices which were three to four millimeter rostral or caudal from the lesion epicenter were picked and photographed with a 10x objective lens using a fluorescence microscope (DP71, Olympus). Images were inverted in black and white and assessed for the number of CGRP-positive immunoreactive pixels with Scion Image. We divided the superficial posterior horn into two layers and deeper regions into three layers for separate measurements.

Quantitative analysis of the GFAP-positive area

We performed GFAP staining to measure the GFAP-positive area eight weeks after SCI. One slide per animal was incubated with mouse anti-GFAP antibody for overnight at 4°C and reacted with Alexa-Fluor 488 goat anti-mouse IgG for one hour at room temperature. Slices were photographed by fluorescent microscopy (DP71, Olympus) using a 4x objective lens. The percentage of the GFAP-positive area was calculated from the number of pixels in the GFAP-positive area divided by the total pixels of the cross sectional area using Scion Image. We calculated the data from three points (the lesion epicenter, 2.5 mm rostral, and 2.5 mm caudal from the lesion

epicenter).

Statistical analysis

The fractional BBB locomotor score, the inclined plane test, the extent of motion (SCANET MV40), and the histological studies were subjected to Student's *t*-test. The time course of recovery of BBB scores was subjected to repeated measures ANOVA followed by *post-hoc* testing using Student's *t*-test. Hypersensitivity of mechanical stimulus and thermal hyperalgesia were subjected to one-way ANOVA followed by Scheffe's *post-hoc* test. Results are presented as mean values ± S.E.M. Values of $p < 0.05$ were considered statistically significant.

Results

Formation of neural stem spheres in ACM

iPS cells grew rapidly on the SNL feeder layer, and remained in an undifferentiated state (Fig. 2A, B). iPS colonies picked up from SNL feeder layers gave rise to floating spheres after four days of cultivation in ACM + FGF-2 (Fig. 2C-F). GFP green fluorescence declined gradually at the surface (Fig. 2G-J). The spheres were composed of three regions. The core region was still undifferentiated, and generated GFP green fluorescence (Fig. 2K). The surface region consisted of neural stem cells (NSCs) which expressed nestin (Fig. 2K white arrows, Fig. 2L), a marker of neural stem cells. The intermediate layer was a transitional stage of differentiation from iPS cells to NSC (Fig. 2K). Subsequently, NSS were cultured in neurobasal medium + FGF-2 and a large number of NSCs migrated from the NSS to the surrounding area (Fig. 2M). After removing NSS from the dish, NSCs were retrieved by trypsin (0.25%) treatment. Retrieved NSCs could be expanded for more than four passages, remaining undifferentiated. We could retrieve 120,000 NSCs from twelve NSS. Thus, one NSS gave rise on average to 10,000 NSCs. Moreover, NSCs could be cryopreserved by a standard protocol.

Differentiation into neurons, astrocytes, and oligodendrocytes

When NSS were transferred to Matrigel-coated plates and cultivated in ACM + FGF-2, Tuj-1-positive neurons migrated from the NSS (Fig. 3A, B). NSS were plated on poly-L-ornithine/fibronectin-coated plates for four days in N2 plus/FGF medium, then N2-plus/FGF/EGF medium for an additional four days, and finally N2 plus/FGF/EGF/PDGF-AA medium for the final four days. Most NSCs then expressed A2B5 (a marker of glial precursor cells) (Fig. 3C). About 30% of A2B5-positive cells differentiated into O4-positive oligodendrocytes after seven days in N2 plus T3 medium (Fig. 3D). High magnification views show that induced oligodendrocytes were both O4 and GalC-positive, stellate-shaped cells (Fig.3E, F). NSCs derived from NSS differentiated exclusively into astrocytes when FGF-2 was removed from neurobasal medium. To differentiate cells into GFAP-positive astrocytes more efficiently, we cultivated NSCs

in DMEM with 10% FBS for 14 days (Fig. 3G). Induced astrocytes had both GFAP and abundant s100 expression in the cytoplasm (Fig. 3H, I).

Gene expression analysis of iPS cells, NSCs, and astrocytes

To investigate gene expression profiles during iPS cellular differentiation into astrocytes, Nanog, *Oct3/4*, nestin, and *GFAP* expression were analyzed quantitatively by RT-PCR. The samples included undifferentiated iPS cells, NSCs (passage number three), and astrocytes differentiated from NSCs (passage number five). Nanog and *Oct3/4* were mainly expressed in iPS cells rather than in NSCs or astrocytes derived from iPS cells (Fig. 4). Nestin expression was upregulated almost two-fold in NSCs compared to astrocytes derived from iPS cells. Conversely, *GFAP* expression was upregulated nearly two-fold in astrocytes derived from iPS cells compared to NSCs.

Behavioral assessments

We transplanted astrocytes derived from iPS cells three and seven days after SCI and measured the BBB locomotor score for eight weeks. The control group received a DMEM injection under the same conditions. There was no statistically significant difference between the astrocyte group and the DMEM group in the BBB locomotor score (repeated-measures ANOVA: three days, p = 0.99, Fig. 5A; seven days, p = 0.115, Fig. 5B).

In the inclined plane test, the three day astrocyte transplant group scored 42.5 ± 1.2 degrees and the three day DMEM group scored 42.5 ± 3.1 degrees. Normal animals averaged 70 ± 0 degrees (n = 5). There was no statistically significant difference between the three day astrocyte transplantation group and the three day DMEM group (p = 1). The extent of locomotion measured by SCANET MV40 for five minutes and 30 minutes also did not show a statistically significant difference (p = 0.84 for five min and p = 0.55 for 30 min, Fig. S1 A and B). The average quantity of locomotion in all groups was 1107.4 ± 138.6 for five min and 2012.5 ± 220.4 for 30 min. Locomotion rapidly slowed in the SCANET box within a few minutes, making it difficult to measure without some stimulus to induce locomotion. These experiments also did not show a statistically significant difference between seven day astrocyte and seven day DMEM groups (data not shown).

Sensory tests

Mechanical thresholds using a dynamic plantar aesthesiometer showed a mean of 41.3 ± 1.7 g in normal rats, decreasing to 21.7 ± 1.6 g in the three day astrocyte transplant group versus 29.5 ± 1.5 g in the three day DMEM control group eight weeks after contusion (Fig. 6A). All contused rats showed more sensitivity to mechanical stimulus than did normal rats (p < 0.001, normal vs. the three day astrocyte group; p = 0.0051, normal versus the three day DMEM group). The three day astrocyte group showed a lower threshold toward mechanical stimulus compared to the

three day DMEM control group ($p = 0.013$). In the seven day transplantation group, mechanical thresholds averaged 25.5 ± 2.7 g versus 28.4 ± 3.3 g in the seven day DMEM group (Fig. 6B). Although all contused rats showed more sensitivity to mechanical stimulus than did normal rats ($p < 0.0066$, normal vs. the seven day astrocyte group; $p = 0.0324$, normal versus seven day DMEM group), there was no statistically significant difference between the seven day astrocyte group and the seven day DMEM group ($p = 0.76$).

Analysis of normal rats with a Hargreaves device revealed a mean thermal latency of 22.3 ± 0 seconds (Fig. 6C) compared to mean values of 17.2 ± 0.9 s in the three day astrocyte group, and 17.8 ± 1.1 s in the three day DMEM group eight weeks after contusion. The three day astrocyte transplant group showed significant thermal hyperalgesia compared to normal rats ($p = 0.018$). In the seven day transplantation group, the mean thermal latency was 16.5 ± 1.6 S and 18.8 ± 1.7 S in the DMEM group. There was no statistical significance ($p = 0.52$). The seven day astrocyte group showed more thermal hyperalgesia compared to normal rats, but the difference did not reach statistical significance ($p = 0.056$).

Histology

Survival of transplanted cells

Transplanted cells labeled with PKH26 red survived eight weeks after transplantation (Fig.7A). These cells fluoresce bright red and stretched their processes in the direction of the longitudinal axis (Fig. 7B, GFAP: green). High magnification images showed that transplanted cells (PKH26 red positive) stretched their process along astrocytes' processes (GFAP: green). Immunofluorescent labeling of GFAP did not co-localize with the PKH26 red fluorescent marker of the transplanted cells (Fig. 7C). Transplanted cells labeled with PKH26 red also did not co-localize with cells marked with the neuronal markers •-tubulin III or GST-•. We counted 69.2 ± 26.2 PKH26-positive transplanted cells / mm^2 in a spinal cord area four mm in length centered on the lesion epicenter. Thus, $\bullet(0.46)^2 \times 69.2 \times 100 = 4598$ cells survived eight weeks after transplantation, or about 4.6% of the original number transplanted. In the seven day astrocyte group, only one rat within three rats processed for sagittal sections had PKH26 red positive transplanted cells in the spinal cord eight weeks after cell transplantation.

White matter sparing

We evaluated the ratio of the retained myelinated area to the whole transverse area of the spinal cord at three points (rostral 2.5 mm from lesion epicenter, lesion epicenter, caudal 2.5 mm from lesion epicenter). There were no statistically significant differences between the controls and animals transplanted at three days at any of the points ($p = 0.91$ for rostral, $p = 0.96$ for lesion epicenter, $p = 0.44$ for caudal, Fig. S2 A-C). We also did not see any statistically significant differences between controls and the animals transplanted after seven days at any points along the spinal cord

(data not shown).

Quantitative analysis of the CGRP-positive area

Supplemental Figure 3 shows CGRP-immunoreactivity 3 - 4 mm rostral from the lesion epicenter (A) and 3 - 4 mm caudal from the lesion epicenter (B) for animals transplanted after three days. We divided the posterior horn into five layers and measured superficial layers (I-II) and deep layers (III-V) in animals receiving astrocytes or DMEM. In the superficial layers, the astrocyte transplant group had greater immunoreactivity for CGRP, but there was no statistical significance to the difference (p = 0.64 for rostral, p = 0.27 for caudal). In deep layers, the CGRP-immunoreactive area was quite limited, and there was no statistically significant difference between the astrocyte group and the DMEM group (p = 0.61 for rostral, p = 0.40 for caudal). We also did not see any statistically significant difference for animals transplanted after seven days at any points along the spinal cord (data not shown).

Quantitative analysis of the GFAP-positive area

Supplemental Figure 4 shows the proportions of the whole cross sectional areas which were GFAP-positive 2.5 mm rostral from the lesion epicenter, at the lesion epicenter, and 2.5 mm caudal from the lesion epicenter. Although the GFAP-positive areas were abundant in the astrocyte groups at all three sites, there were no statistically significant differences (p = 0.09 for rostral, p = 0.79 for lesion epicenter, and p = 0.27 for caudal).

Discussion

The present study consisted of two parts. In the first portion, we documented that the NSS method can successfully differentiate mouse iPS cells into astrocytes. In the second portion of the study, we described the results obtained by transplanting iPS-derived cells into SCI lesions.

NSS method for iPS cell differentiation

Several methods have been developed to prepare neural cells from ES cells. These include the use of embryoid bodies,[32] induction via retinoic acid,[1] and the use of stromal cell-derived inducing activity (SDIA).[18] Nakayama *et al.* reported that astrocyte-derived factors can mediate differentiation of ES cells into neurons.[27] They also described a NSS method in which FGF-2 was withdrawn from medium leading NSCs to differentiate into astrocytes.[29,30] Differentiation of neurons from ES cells using the NSS method is well established. Using the NSS method, dopaminergic neurons have been derived from monkey ES cells and have been transplanted to monkeys with Parkinson's disease, resulting in improved motor function.[24] Human neurons, generated from ES cells by the NSS method, survive in murine brains following xenotransplantation.[34] Nakayama reported that the NSS method was very efficient because each ES cell generated 1000 NSCs over 11 days.[28] Moreover, xeno-free induction is possible because chemically defined N2

medium can generate NSS without having to resort to rodent ACM.[34] We hypothesized that the NSS method could be applied to iPS cell differentiation. In the present study, we transferred iPS cell colonies to floating cultures, and differentiated NSCs on the surface of the NSS. NSCs rapidly migrated away after the shift to adhesion culture. We could propagate NSCs in this fashion, followed by cryopreservation. NSCs were successfully differentiated into astrocytes, neurons, and oligodendrocytes. The results of quantitative RT-PCR study were reasonable because GFAP transcripts were more abundant in the astrocytes derived from iPS cells than in the NSCs. We also showed that astrocytes derived from iPS cells have abundant S-100 and GFAP proteins in the cytoplasm.

Recently, two papers demonstrated that human pluripotent stem cells could differentiate into oligodendrocytes[14] or spinal motor neurons.[13] They showed that neural cells could be differentiated by way of neuroepithelial cells over more than two months. Okuno *et al.* demonstrated that human ES cells could differentiate into neural cells within one month by the NSS method.[34] We emphasize that the NSS method could be quite rapid if applied clinically. Additional advantages of the NSS method include obtaining NSCs with high purity and the option of cryopreservation. The generation of NSCs from NSS is efficient and a useful option for regenerative medicine. Neural progenitors were produced from murine ES cells by a combination of non-adherent conditions and serum starvation.[21] They showed that stem cell markers Oct4 and Nanog decreased and nestin increased after differentiation of ES cells to neural progenitors in floating spheres as in the present study. While the sphere-like structures resembled those observed in the present study, the proliferation efficacy of neural progenitor cells remains unclear. The generation of NSCs from NSS is still efficient and is a useful option for regenerative medicine.

Astrocyte transplantation causes greater sensitivity to mechanical stimulus

Astrocytes derived from iPS cells were injected into rat spinal cord lesions three and seven days after SCI. Although the astrocyte group did not show locomotor recovery that was significantly better than the DMEM group, transplanted cells survived in the spinal cords eight weeks after transplantation. Transplanted astrocytes changed their character to GFAP-negative cells in the injured spinal cord eight weeks after transplantation. Astrocyte transplantation increased the recipients' sensitivity to mechanical stimulus and thermal hyperalgesia compared to normal rats. Also, three day astrocyte transplantation caused greater sensitivity to mechanical stimulus compared to DMEM controls. Greater sensitivity to mechanical stimulus is mainly caused by reactive astrocytes, perhaps through the secretion of diffusible chemical transmitters which may augment primary afferent neuronal signaling or sensitize second order neurons in the spinal cord.[11] Transplanted astrocytes

derived from glial precursors induced allodynia after SCI.[5] Transduction of neural stem cells with neurogenin-2 before transplantation suppressed astrocytic differentiation of engrafted cells and prevented graft-induced sprouting and allodynia.[12] These reports support our finding that astrocytes derived from iPS cells caused greater sensitivity to mechanical stimulus. Neural stem cell transplantation also causes allodynia of the forelimbs after thoracic SCI without functional recovery.[22] The onset of allodynia might be a general occurrence because it is difficult to envision a causal association between forelimb allodynia and thoracic SCI.

Early astrocyte transplantation

In the present study, early astrocyte transplantation alone did not promote motor recovery as described above. We expected cell survival factors, like neurotrophins, would be up-regulated by astrocyte transplantation, leading to improved salvage of neuronal cells. We were unable to demonstrate a statistically significant difference in white matter sparing using Luxol fast blue staining. Thus, early transplantation of astrocytes to save damaged tissue at the lesion epicenter did not show the expected results. Many studies have reported that the transplantation of NSCs promotes motor recovery.[16,31] Possible mechanisms of recovery include remyelination by oligodendrocytes differentiated from transplanted NSCs,[3,19] and donor-derived immature neurons forming both efferent and afferent synapses with host neurons.[3,37] In the present study, iPS-derived astrocytes changed their character to GFAP-negative cells after transplantation and contacted GFAP-positive host astrocytes. Trans-differentiation of transplanted cells in the injured spinal cord could explain their change in function. In the present study, approximately 5% of the 100,000 cells injected into the injured spinal cord survived eight weeks. Immediately after injury, the levels of many neurotoxic inflammatory cytokines (such as interleukin (IL)-1, IL-6, and tumor necrosis factor (TNF)-alpha) increase and then decline sharply within 24 hr.[26] When neurosphere-derived neural progenitor cells were transplanted 24 hr after the injury, almost none of the grafted cells survived.[31] Transplanted cells could be damaged by inflammatory cytokines after cell transplantation. Thus, astrocyte transplantation did not proceed as anticipated in the injured spinal cord. These results suggest that iPS-derived astrocyte transplantation three and seven days after SCI is insufficient to achieve locomotor recovery. In the setting of traumatic SCI, neurons, oligodendrocytes, and astrocytes are damaged simultaneously. Karimi et al. reported that adult neural stem/ progenitor cell transplantation with Chondroitinase and growth factor improved functional recovery.[17] We conclude that transplanting a single type cell for spinal cord injury is insufficient to improve functional recovery. On the other hand, a critical aspect of regenerative medicine is guaranteeing the safety of the patient. In that regard, we suggest that the NSS method, which is quite simple and efficient, could be utilized

with confidence.

Conclusions

Astrocytes derived from iPS cells were injected into rat spinal cord lesions three and seven days after SCI. Although the astrocyte group did not show significantly better locomotor recovery than the DMEM group, transplanted cells survived in the spinal cords eight weeks after transplantation. Astrocyte transplantation increased the recipients' sensitivity to mechanical stimulus compared to DMEM controls. We conclude that transplanting astrocytes differentiated by serum treatment of neural stem cells (generated from iPS cell-derived, neural stem spheres), is poorly suited for repairing SCI.

Acknowledgements

We thank Dr. Michiyo Terashima at Hokkaido University, Japan for technical assistance. This research was supported by a grant-in-aid for Japanese scientific research grant 19591715.

Disclosure

The authors report no conflict of interest concerning the materials or methods used in this study or the findings specified in this paper.

References

1. Bain G, Kitchens D, Yao M, Huettner JE, Gottlieb DI: Embryonic stem cells express neuronal properties in vitro. Dev Biol 168: 342-57, 1995

2. Basso DM, Beattie MS, Bresnahan JC: A sensitive and reliable locomotor rating scale for open field testing in rats. J Neurotrauma 12: 1-21, 1995

3. Cummings BJ, Uchida N, Tamaki SJ, Salazar DL, Hooshmand M, Summers R, et al: Human neural stem cells differentiate and promote locomotor recovery in spinal cord-injured mice. Proc Natl Acad Sci U S A 102: 14069-74, 2005

4. Davies JE, Huang C, Proschel C, Noble M, Mayer-Proschel M, Davies SJ: Astrocytes derived from glial-restricted precursors promote spinal cord repair. J Biol 5: 7, 2006

5. Davies JE, Pröschel C, Zhang N, Noble M, Mayer-Pröschel M, Davies SJ: Transplanted astrocytes derived from BMP- or CNTF-treated glial-restricted precursors have opposite effects on recovery and allodynia after spinal cord injury. J Biol 7: 24, 2008

6. Davies SJ, Fitch MT, Memberg SP, Hall AK, Raisman G, Silver J: Regeneration of adult axons in white matter tracts of the central nervous system. Nature 390: 680-3, 1997

7. Davies SJ, Goucher DR, Doller C, Silver J: Robust regeneration of adult sensory axons in degenerating white matter of the adult rat spinal cord. J Neurosci 19: 5810-22, 1999

8. Desclaux M, Teigell M, Amar L, Vogel R, Gimenez Y, Ribotta M, et al: A novel and efficient gene transfer strategy reduces glial reactivity and improves neuronal survival and axonal growth in vitro. PLoS One 4: e6227, 2009

9. Faulkner JR, Herrmann JE, Woo MJ, Tansey KE, Doan NB, Sofroniew MV: Reactive astrocytes protect tissue and preserve function after spinal cord injury. J Neurosci 24: 2143-55,

2004

10. Fawcett JW, Asher RA: The glial scar and central nervous system repair. Brain Res Bull 49: 377-391,1999

11. Hald A: Spinal astrogliosis in pain models: cause and effects. Cell Mol Neurobiol 29: 609-19, 2009

12. Hofstetter CP, Holmström NA, Lilja JA, Schweinhardt P, Hao J, Spenger C, et al: Allodynia limits the usefulness of intraspinal neural stem cell grafts; directed differentiation improves outcome. Nat Neurosci 8: 346-53, 2005

13. Hu BY, Zhang SC: Differentiation of spinal motor neurons from pluripotent human stem cells. Nat Protoc 4: 1295-304, 2009

14. Hu BY, Du ZW, Zhang SC: Differentiation of human oligodendrocytes from pluripotent stem cells. Nat Protoc 4: 1614-22, 2009

15. Iseda T, Nishio T, Kawaguchi S, Yamanoto M, Kawasaki T, Wakisaka S: Spontenious regeneration of the corticospinal tract after transaction in young rats: a key role of reactive astrocytes in making favorable and unfavorable conditions for regeneration. Neuroscience 126: 365-374, 2004

16. Iwanami A, Kaneko S, Nakamura M, Kanemura Y, Mori H, Kobayashi S, et al: Transplantation of human neural stem cells for spinal cord injury in primates. J Neurosci Res 80: 182-90, 2005

17. Karimi-Abdolrezaee S, Efynergistic effects of transplanted adult neural stem/ progenitor cells, chondroitinase, and growth factors promote functional repair and plasticity of the chronically injured spinal cord. J Neurosci 30: 1657-1676, 2010

18. Kawasaki H, Mizuseki K, Nishikawa S, Kaneko S, Kuwana Y, Nakanishi S, et al: Induction of midbrain dopaminergic neurons from ES cells by stromal cell-derived inducing activity. Neuron 28: 31-40, 2000

19. Keirstead HS, Nistor G, Bernal G, Totoiu M, Cloutier F, Sharp K, et al: Human embryonic stem cell-derived oligodendrocyte progenitor cell transplants remyelinate and restore locomotion after spinal cord injury. J Neurosci 25: 4694-705, 2005

20. Lemons ML, Howland DR, Anderson DK: Chondroitin sulfate proteoglycan immunoreactivity increases following spinal cord injury and transplantation. Exp Neurol 160: 51-65, 1999

21. Li H, Liu H, Corrales CE, Risner JR, Forrester J, Holt JR, et al: Differentiation of neurons from neural precursors generated in floating spheres from embryonic stem cells. BMC Neurosci 10: 122, 2009

22. Macias MY, Syring MB, Pizzi MA, Crowe MJ, Alexanian AR, Kurpad SN: Pain with no gain: allodynia following neural stem cell transplantation in spinal cord injury. Exp Neurol 201: 335-48, 2006

23. Mikami Y, Toda M, Watanabe M, Nakamura M, Toyama Y, Kawakami Y: A simple and reliable behavioral analysis of locomotor function after spinal cord injury in mice. Technical note. J Neurosurg 97: 142-7, 2002

24. Muramatsu S, Okuno T, Suzuki Y, Nakayama T, Kakiuchi T, Takino N, et al: Multitracer Assessment of Dopamine Function

After Transplantation of embryonic stem cell-derived neural stem cells in a primate model of Parkinson's disease. Synapse 62: 541-548, 2009

25. Myer DJ, Gurkoff GG, Lee SM, Hovda DA, Sofroniew MV: Essential protective roles of reactive astrocytes in traumatic brain injury. Brain 129: 2761-2772, 2006

26. Nakamura M, Houghtling RA, MacArthur L, Bayer BM, Bregman BS: Differences in cytokine gene expression profile between acute and secondary injury in adult rat spinal cord. Exp Neurol 184: 313-25, 2003

27. Nakayama T, Motoki-Soga T, Inoue N: Astrocyte-derived factos instruct differentiation of embryonic stem cells into neurons. Neurosci Res 46: 241-249, 2003

28. Nakayama T, Motoki-Soga T, Yamaguchi K, Inoue N: Efficient production of neural stem cell and neurons from embryonic stem cells. NeuroReport 15: 487-491, 2004

29. Nakayama T, Inoue N: Neural stem sphere method: induction of neural stem cells and neurons by astocyte-derived factors in embryonic stem cells in vitro. Method Mol Biol 330: 1-13, 2008

30. Nakayama T, Sai T, Otsu M, Momoki-Soga T, Inoue N: Astrocytogenesis of embryonic stem-cell-derived neural stem cells: default differentiation. NeuroReport 17: 1519-1523, 2006

31. Ogawa Y, Sawamoto K, Miyata T, Miyao S, Watanabe M, Nakamura M, et al: Transplantation of in vitro-expanded fetal neural progenitor cells results in neurogenesis and functional recovery after spinal cord contusion injury in adult rats. J Neurosci Res 69: 925-33, 2002

32. Okabe S, Forsberg-Nilsson K, Spiro AC, Segal M, McKay RD: Development of neuronal precursor cells and functional postmitotic neurons from embryonic stem cells in vitro. Mech Dev 59: 89-102, 1996

33. Okada S, Nakamura M, Katoh H, Miyao T, Shimazaki T, Ishii K, et al: Conditional ablation of Stat3 or Socs3 discloses a dual role for reactive astrocytes after spinal cord injury. Nat Med 12: 829-834, 2006

34. Okuno T, Nakayama T, Konishi N, Michibata H, Wakimoto K, Suzuki Y, et al: Self-contained induction of neurons from human embryonic stem cells. PLoS One 4: e6318, 2009

35. Takahashi K, Yamanaka S: Induction of pluripotent stem cells from mouse embryonic and adult fibroblast cultures by defined factors. Cell 126: 663-76, 2006

36. Takahashi K, Tanabe K, Ohnuki M, Narita M, Ichisaka T, Tomoda K, et al: Induction of pluripotent stem cells from adult human fibroblasts by defined factors. Cell 131: 861-72, 2007

37. Uchida K, Okano H, Hayashi T, Mine Y, Tanioka Y, Nomura T, et al: Grafted swine neuroepithelial stem cells can form myelinated axons and both efferent and afferent synapses with xenogeneic rat neurons. J Neurosci Res 72: 661-9, 2003

38. Voskuhl RR, Peterson RS, Song B, Ao Y, Morales LB, Tiwari-Woodruff S, et al: Reactive astrocytes form scar-like perivascular barriers to leukocytes during adaptive immune

inflammation of the CNS. J Neurosci 29: 11511-22, 2009

Figure legends

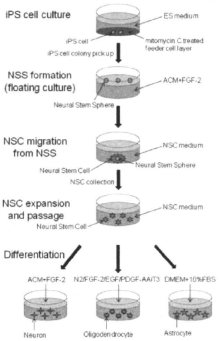

Fig. 1. Schema of the NSS method.
iPS cells were differentiated into neurons, oligodendrocytes, and astrocytes via NSCs.

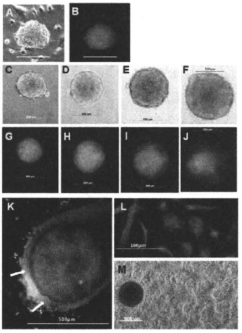

Fig. 2. Formation of NSS from mouse iPS cells.

A, B. iPS cells formed colonies on the feeder layer. Bright field (A) and dark field (B) show that iPS cells aggregated and formed 300 - 500 μm undifferentiated iPS colonies. GFP green fluorescence shows undifferentiated conditions (B). Bar = 500 μm.

C-J. Colony picked from a feeder layer grew gradually over four days in nonadherent culture in ACM + FGF-2 (C - F). GFP green fluorescence signals were reduced at the surface in spite of increasing colony size (G - J). Bar = 500 μm.

K-L. Fluorescent images of NSS. K, Overall staining for NSS shows that the core contained undifferentiated cells (GFP green) and the peripheral cells expressed nestin (red, white arrows), a marker of differentiated NSC. The intermediate region represents a transitional state. DAPI was used for nuclear staining (blue). L, Peripheral area has many nestin-positive NSC. M, Low magnification image of phase-contrast micrograph shows many NSC had migrated radially from NSS during the adherent stage in neural basal medium + FGF-2 at day 10.

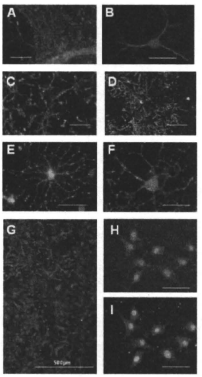

Fig. 3. NSC differentiation into neurons, oligodendrocytes, and astrocytes.

A, B. NSS were plated on Matrigel-coated dishes and cultivated for five days in NSC medium. Many neurons (Tuj-1, red) migrated from NSS (A, Bar = 100 μm). High magnification image shows that Tuj-1-positive neurons stretched their axons and dendrites from the cell body (B, Bar = 50 μm).

C, D. Expanded NSCs differentiated into oligodendrocytes during 21 days of culture. C, Expanded NSCs were cultivated for 12 days per the manufacturer's protocol. Most cells became A2B5-positive (A2B5, green). Bar = 200 μm. D, Subsequently, the medium was changed to N2 plus/T3 medium, and the cells were cultivated for an additional seven days. Approximately 30% of the cells differentiated into oligodendrocytes (O4, green). Bar = 100 μm.

E, F. High magnification images of differentiated oligodendrocytes (E: O4, F: GalC). Bar = 50 μm.

G-I. Expanded NSC were plated on PLL-coated dishes and cultivated in DMEM with 10% FBS without FGF-2 for 14 days. Almost all cells differentiated into GFAP-positive astrocytes (GFAP, green) (G). Bar = 500 μm.

H,I. High magnification images of differentiated astrocytes. Derived astrocytes were double-positive for GFAP (H, green) and s100 (I, red). Bar= 50μm.

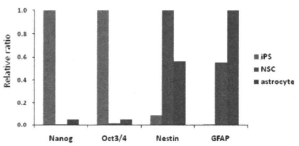

Fig. 4. Gene expression analysis by real time RT-PCR.

Gene expression of *Nanog, Oct3/4,* nestin, *and GFAP* were normalized by *GAPDH* mRNA for each cell phenotype (iPS cells, NSCs, and astrocytes) and data were plotted in a bar graph. *Nanog* and *Oct3/4* were highly upregulated only in iPS cells. Nestin was upregulated in NSC rather than astrocytes. *GFAP* was upregulated in astrocytes compared to NSCs. iPS cells showed low expression of both nestin and *GFAP*.

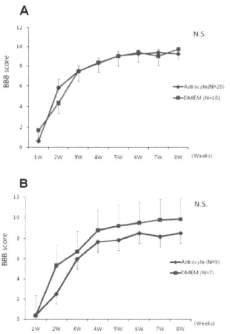

Fig. 5. Functional assessment of the hindlimb with BBB locomotor score.

A. There was no statistically significant difference between the three day astrocyte group and the three day DMEM group in BBB locomotor scores (repeated measures ANOVA, $p = 0.99$).

B. Although the BBB locomotor score of the seven day astrocyte group was always less than that of the seven day DMEM group, there was no statistically significant difference between them (repeated measures ANOVA, $p = 0.115$).

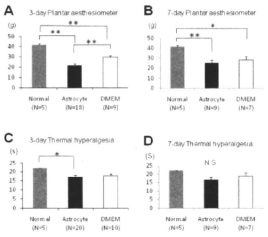

Fig. 6. Sensory tests

A, B. Mechanical withdrawal thresholds in rat hind limbs were tested using a dynamic plantar aesthesiometer. SCI significantly decreased thresholds of mechanical stimulus compared to those of normal rats (**A, B**). Astrocyte transplantation three days after SCI significantly decreased thresholds of mechanical stimulus compared to DMEM injection (**A,** $^{**}p < 0.01$).

C, D. Thermal nociceptive thresholds in rat hind limbs were evaluated using a Hargreaves device. Astrocyte transplantation three days after SCI significantly decreased thermal nociceptive thresholds compared to normal rats (**C,** $^{*}p < 0.05$). The seven day astrocyte group showed more thermal hyperalgesia compared to normal rats, but the difference did not reach statistical significance (**D,** $p = 0.056$).

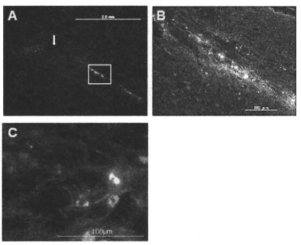

Fig. 7. Transplanted cells labeled with PKH26 survived eight weeks after transplantation.

A. Low magnification images show transplanted (red) cells had migrated more than four mm toward the long axis of the spinal cord (Bar = 2.0 mm). White arrow indicates lesion epicenter. **B.** High magnification image of white box area in (A). Transplanted cells stretched their processes toward the longitudinal axis in the spinal cord (GFAP, green; Bar = 200 μm). **C.** High magnification images, sagittal views, show transplanted (red) cells stretched their processes along astrocyte processes (GFAP, green). DAPI was used for nuclear staining (Blue). Processes did not merge (Bar = 100 μm).

Supplemented figure legends

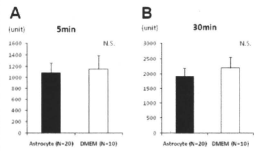

Fig. S1. SCANET MV40 movement analysis

A, B. In SCANET MV40 movement analysis for three day transplantation, neither group showed a statistically significant difference in movement during five (A) and 30 min (B) observation periods.

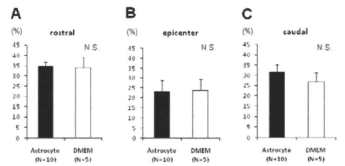

Fig. S2. Evaluation of remaining myelinated area by LFB staining for three day transplantation

A-C, We evaluated the ratio of remaining myelinated area to the whole transverse section at three sites along the spinal cord (A, rostral 2.5 mm from lesion epicenter; B, lesion epicenter; C, caudal 2.5 mm from lesion epicenter). There was no statistically significant difference between astrocyte and DMEM groups at any of the sites.

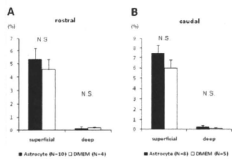

Fig. S3. Quantitative analysis of CGRP-positive area for three day transplantation

A, B, In spinal cord cross sections, CGRP-immunoreactivity was measured (as pixels) in areas 3 - 4 mm rostral (A) and 3 – 4 mm caudal (B) for superficial and deep layers. There were no statistically significant differences in any of the layers at rostral and caudal sites between astrocyte and DMEM groups.

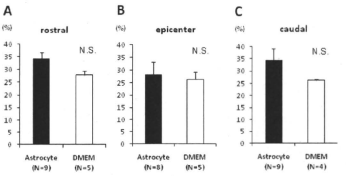

Fig. S4. Quantitative analysis of GFAP-positive area

A-C, GFAP-immunoreactive areas were measured (as pixels) in spinal cord cross sections at 2.5 mm rostral (A), lesion epicenter (B), and 2.5 mm caudal (C). There were no statistically significant differences at any of the sites between astrocyte and DMEM groups.

Pathophysiology of the damaged spinal cord seen in the autopsy of a woman nine years after operation for severe cervical spondylotic myelopathy

Yukio Someya[1], Masao Koda[1], Masayuki Hashimoto[1], Akihiko Okawa[1], Yutaka Masaki[1], Masashi Yamazaki[1].

[1]Department of Orthopaedic Surgery, Graduate School of Medicine, Chiba University

Corresponding author: Masayuki Hashimoto
Department of Orthopaedic Surgery, Graduate School of Medicine, Chiba University
1-8-1 Inohana, Chuo-ku, Chiba 2608670, Japan.
Tel: +81-43-226-2117, Fax: +81-43-226-2116, E-mail: futre@tg7.so-net.ne.jp

Abstract

Context: We report the autopsy of a 65-year-old woman who underwent a C3–7 laminoplasty for cervical spondylotic myelopathy four years from onset. Her sensory disturbance, spasticity, and vesicorectal disturbance, which were corresponded to long tract sign was improved in spite of unchanged activities of daily living.

Findings: Cross sections at the C4–5 level showed a triangular shape because of atrophied ventral gray matter. Moreover, despite the scarce glial scar formation around the cystic cavity, regeneration of gray matter had not occurred. In the white matter, the posterior and lateral funiculi were shrunken including three to four segments.

Conclusion: Pathological change of white matter did not coincide with clinical symptoms in the present case that long tract sign caused by a white matter lesion was reactive to treatment. From the findings of the present study we believe that it is better to operate earlier in cases of cervical spondylotic myelopathy, because delay of surgery may be responsible for irreversible histological change.

Key Words: pathology; cervical spondylotic myelopathy; autopsy; laminoplasty; long tract sign

Introduction

Reports of the pathology of cervical spondylotic myelopathy (CSM) are rare because it is not a fatal disorder (1,2,3,4,5,6). Autopsy study of patients who have undergone laminoplasty for CSM are scarce. Here we report the autopsy of a woman who had a C3–7 laminoplasty for a case of CSM nine years ago.

Clinical summary

History

The woman was a 65-year-old who

had multiple joint contractures caused by rheumatoid arthritis (stage IV class 4) for more than 30 years and barely ambulated using a walker. She had noticed progressive weakness in her bilateral lower extremities at 52 years of age and she was diagnosed as having cervical spondylotic myelopathy. She gradually suffered from right-sided muscle weakness and spasticity of her bilateral lower extremities and became confined to a wheelchair. She felt sensory disturbance on the left side of her body trunk and extremities, and had to urinate frequently four years from the onset of symptoms. She decided to undergo a C3–7 laminoplasty at 56 years of age. She was satisfied with the results of her operation, because her sensory disturbance, spasticity, and vesicorectal disturbance were improved in spite of unchanged activities of daily living (ADL). She died nine years after the operation at 65 years of age because of an acute mitral infarction.

Imaging

Plain X-ray imaging and MRI one year after her operation showed sufficient surgical decompression (Fig. 1 and 2A). Sagittal views of her spinal cord showed low intensity in T1-weighted images and high intensity in T2-weighted images at the level of C4–5, and an axial view showed a snake-eyed appearance at that site (Fig 2B).

Pathological findings

Transplanted bone was fused with innate bone and we could not find instability at any disc level. Macroscopically, dissected spinal cord had atrophy at the level of C4–C5, as seen on MRI. In spite of a formalin-fixed sample, spinal cord tissue was sufficiently degenerated to be unstable at the level of C4–C5.

We stained spinal cord cross sections with hematoxylin and eosin (H&E), Luxol fast blue (LFB) and elastica van Gieson (EVG), and performed immunohistochemistry for GFAP. Cross sections at the level of C4–C5 were a triangular shape because anterior horn neurons that had formerly undergone atrophy were lost in the ventral gray matter. Moreover, tissue was sufficiently degenerated to form a cystic cavity at the center of the gray matter of the posterior horn and funiculus (Fig. 3A, D). Atrophy of gray matter had spread vertically from the C6 to C7 segments (Fig. 3B, C). A cystic cavity was consistent with the snake-eyed appearance of the axial view on T2-weighted MRI. GFAP staining showed that the glial reaction was comparatively rare around the cystic cavity (Fig. 4). Vessels adjacent to the cystic cavity had a thickened outer membrane with hyaline degeneration. These vessels were lacking elastic fiber and had dilated or occluded lumens (Fig. 5). In the white matter, the posterior and lateral funiculi were shrunken and stained weakly with LFB (Fig. 3A). Their atrophy spread for 3 to 4 segments, predominantly on the right side (Fig. 3B, C). The anterior funiculus remained comparatively intact compared with the posterior or lateral funiculus. Its atrophy had only spread within two segments. These findings of substance changes

were predominantly in the right side of the spinal cord.

Discussion

In CSM, disease onset is related to secondary circulatory disturbance with static or dynamic compression (7). It is reported that chronic venous congestion is a cause of vessel changes (8). Kameyama reports that some cysts had surrounding intact neurons, were disrupted alongside vessels, or had many thickened vessels in them. He speculated that cysts formed from fused enlarged perivascular spaces caused by congestion and edema (9). In the present pathology, we found many thickened vessels adjacent to the cystic cavity, with fibrotic changes and enlargement of their perivascular space. These findings were coincided with the findings of chronic congestion caused by spinal cord compression.

In the present case, the cystic cavity had spread from the center of the gray matter to the posterior horn and funiculus. This phenomenon is explained by shear stress, which increases towards the middle and becomes highest in the center of the spinal cord (10). It is reported that the center of gray matter, posterior, and lateral funiculus are most subject to severe compression in CSM (6). From this description, the location of the cystic cavity is reasonable in the present case.

Before surgery, she had sensory disturbance of her body trunk, lower extremities, spasticity, hyper-reflexes, and vesico-rectal disturbance, which may have been caused by long tract disturbance. After surgery, MMT score of her right side lower extremity increased to 3. She was satisfied that her sensory disturbance, spasticity, and vesico-rectal disturbance, which were related to the long tract sign, had improved. Although it is expected that many axons were reconnected or regenerated after decompressive surgery, the posterior and lateral funiculi were shrunken and atrophied ranged 3 to 4 segments. Ito reported the existence of thinned myelin sheaths in an autopsy case of CSM and postulated the possibility of demyelination and remyelination (2). In the present case, pathological findings were not corresponded with clinical symptoms that the long tract sign caused by the white matter lesion were responded to treatment.

References

1. Hawkins JC 3rd, Yaghmai F, Gindin RA. Cervical myelopathy due to spondylosis. Case report. *J Neurosurg.* 1978; 48:297-301.

2. Ito T, Oyanagi K, Takahashi H, Takahashi HE, Ikuta F. Cervical spondylotic myelopathy. Clinicopathologic study on the progression pattern and thin myelinated fibers of the lesions of seven patients examined during complete autopsy. *Spine* 1996; 21:827-33.

3. Kameyama T, Ando T, Yanagi T, Hashizume Y. Neuroimaging and pathology of the spinal cord in compressive cervical myelopathy: Review. *Rinsho Byori* 1995; 43:886-90 (Jpn).

4. Mizuno J, Nakagawa H, Inoue T, Hashizume Y. Clinicopathological study of "snake-eye appearance" in compressive

myelopathy of the cervical spinal cord. *J Neurosurg*. 2003; 99(2 Suppl):162-8.

5. Nakano KK, Schoene WC, Baker RA, Dawson DM. The cervical myelopathy associated with rheumatoid arthritis: analysis of patients, with 2 postmortem cases. *Ann Neurol*. 1978; 3:144-51.

6. Ogino H, Tada K, Okada K. et al. Canal diameter, anteroposterior compression ratio, and spondylotic myelopathy of the cervical spine. *Spine* 1983; 8:1-15.

7. Baptiste DC, Fehlings MG. Pathophysiology of cervical myelopathy. *Spine J* 2006; 6 (6 Suppl):190S-197S.

8. Kameyama T, Hashizume Y. Clinicopathology of cervical spondylotic myelopathy. *No no Kagaku* 2003; 25: 767-775 (Jpn).

9. Kameyama T, Hashizume Y, Sobue G. Neuropathology of spinal cord cyst in cervical compression myelopathy. *Japan OPLL research study group* 1996; 168-172 (Jpn).

10. Panjabi M, White A. Biomechanics of nonacute cervical spinal cord trauma. *Spine* 1998; 13:838-842.

Figure legends

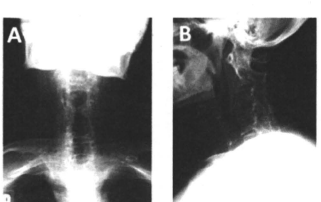

Figure 1

Cervical X-ray one year after C3–7 laminoplasty (A: Anterior–posterior view, B: Profile view).

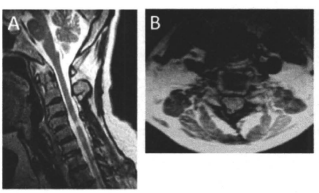

Figure 2

MRI findings one year after C3–7 laminoplasty (A: T2-weighted sagittal view, B: T2-weighted axial view). Although subdural space is widely decompressed in the sagittal view, the high intensity area at the level of C4/5 remains (A). In the axial view of the spinal cord at the level of C4/5, the gray matter shows a snake-eyed appearance, where the high intensity area is predominant (B).

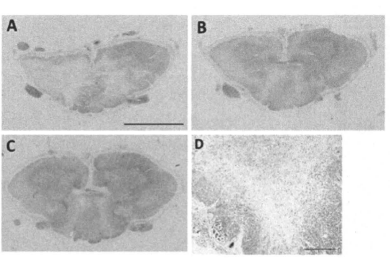

Figure 3

Luxol fast blue (LFB) staining of a cross section of the cervical spinal cord (A–C) and hematoxylin and eosin (H&E) staining of a serial section of A (D). Fig. 3A, B, and C correspond with cross sections at C4/5, C5/6,